2.0 FINAL PRETEST ANALYSIS

2.1   Scope of Final Pretest Analysis

Pretest prediction analysis of the NUPEC/SNL 1:4 scale PCCV model LST is formally documented in the NUREG CR-6685 Report [1]. Due to the logistics of report preparation and reviewing requirements, the analyses reported therein were performed in the fall of 1999, one year prior to the LST scheduled for September, 2000. A final set of pretest prediction analyses were performed just prior to the test, which incorporated updated properties and in-situ conditions of the model. These final pretest analyses were performed primarily to support test operations by providing the 'best' predictions of the model's response for real-time comparison with the actual response. This information was essential to the safe and successful conduct of the test. The properties and modeling inputs considered for modification were:

1.   Concrete material properties,
2.   Prestress (stress levels, stress distribution due to friction, and anchor set), and
3.   Creep, temperature, and other time dependent effects.

The global axisymmetric, the semi-global 3DCM models, and the local penetration models were reanalyzed. The local failure predictions are all driven by response versus pressure histories calculated by the 3DCM model, but the local models had to be reanalyzed to save the data recently selected for monitoring during the test. How the updated modeling inputs were considered in the final analyses is summarized herein.

2.2 Final Model Inputs

2.2.1 Concrete Material Properties

Because visual inspection of the model reveals the existence of microcracking (probably due to curing and shrinkage) throughout the cylinder, the concrete tensile strength was reduced to correspond to a cracking strain of $\varepsilon_{cr} = 40. \times 10^{-6}$. This is half of the value used in the prior analysis.

A new suite of concrete compressive tests conducted at Construction Technology Laboratories (CTL) became available in February, 2000. The concrete pour designations are shown in Figure 2-1 and the latest test results are tabulated in the CTL test excerpt, Table 2-1. How this data was used in the reanalysis is summarized below.

2.2.1.1 Axisymmetric Analysis
Based on prior analysis, the areas where concrete behavior most influences model behavior are in regions C1 and F3B. A third zone, the rest of the basemat, was also identified separately because of the differences in material specifications for this zone. The zones used for the analysis assumptions are shown in Figure 2-1. The average strengths and moduli assigned for these regions are as follows:

		Region C1	Region F3B	Rest of Basemat
f_c'	=	60.9 MPa (8831 psi)	59.4 MPa (8613 psi)	49.2 MPa (7,134 psi)
E	=	27.1 GPa ($3.93 \cdot 10^6$ psi)	28.0 GPa (4.06×10^6 psi)	26.0 MPa (3.77×10^6 psi)

These figures were computed by averaging the data in Table 2-1, but only using "C1," "F3B," and the average of region "F1," "F2," and "F3A," respectively. The Region C1 and F3B strengths are roughly 22% higher than what was used in the prior prediction analysis, and may, therefore, have a noticeable effect on the cylinder wall flexural behavior. The Young's Moduli are roughly 15% lower than what was used in the prior analysis. Note that the strain at peak stress (provided in e-mail correspondence from M. F. Hessheimer, 7/21/00) is mostly in the range of 0.0025 to 0.0026, so the shape of the stress-strain curve used in the prior analysis is judged to be reasonable with the exception of softening the modulus.

Table 2-1. Strength and Modulus of Elasticity Results

Sample	Test Number	Load, kN	Stress MPa	Average	Modulus GPa	Average
C1T2	4	1,077	59.0	60.9	26.0	27.1
C1T5	1	1,146	62.8		28.2	
C1T6	3	1,109	60.8		27.2	
C2T1	7	1,142	62.6	57.0	25.5	26.6
C2T3	5	959	52.6		26.0	
C2T4	6	1,019	55.9		28.3	
C3T1	8	961	52.7	50.7	18.4	24.4
C3T3	9	1,101	60.4		29.5	
C3T5	2	711	39.0		25.3	
C4T1	11	1,151	63.1	61.8	28.6	28.6
C4T2	10	1,302	71.4		32.4	
C4T3	12	930	51.0		24.9	
D1T2	13	1,316	72.1	71.3	30.8	30.9
D1T3	14	1,293	70.9		30.9	
D1T4	15	1,291	70.8		31.1	
D2T2	16	977	53.6	50.7	28.0	23.6
D2T3	17	799	43.8		15.9	
D2T4	18	996	54.6		26.9	
D3T1	19	1,322	72.5	57.0	31.6	22.5
D3T2	20	873	47.8		17.3	
D3T2	21	922	50.6		18.6	
F1T5	32	1,045	57.3	52.2	22.0	25.8
F1T6	31	1,010	55.3		28.3	
F1T8	33	803	44.0		27.2	
F2T2	30	978	53.6	54.2	27.2	29.5
F2T4	29	911	49.9		28.2	
F2T8	28	1,078	59.1		33.2	
F3AT3	35	790	43.3	41.2	26.4	22.8
F3AT4	36	628	34.4		16.0	
F3AT5	34	839	46.0		26.0	
F3BT2	25	1,316	72.1	59.4	30.6	28.0
F3BT3	26	920	50.4		26.8	
F3BT7	27	1,017	55.8		26.7	
F4T1	22	1,239	67.9	65.9	29.1	30.0
F4T2	23	1,161	63.6		30.2	
F4T2	24	1,205	66.0		30.5	

If all the cylinder and dome pours were averaged, then

$$f'_{c_{avg}} = 58.5 \text{MPa}$$

which is within 4% of the C1 value. For this reason, it was decided to use the C1 value throughout the cylinder and dome of the axisymmetric analysis. Similarly, the average value for the basemat is 54.6 MPa or within 8% of the F3B value; therefore, it was decided to use the F3B value, as shown.

2.2.1.2 3DCM Analysis

The 3DCM model encompasses all of region C3 (whose strength is substantially lower than C1) and about half of region C4. For this model, the compressive properties were modified as follows:

$$f'_c = \left(f'_{c_{e3}} + 0.5 f'_{c_{e4}} \right) / 1.5 = 54.4 MPa \left(7{,}838 \ psi \right)$$

$$E = \left(E_{c3} + 0.5 E_{c4} \right) / 1.5 = 25.8 GPa \left(3.74 x 10^6 \ psi \right)$$

2.2.2 Prestressing

Table 2-2 shows a prestressing data summary, prepared by SNL, which tabulates the averages for measurements of forces, friction, and seating losses.

Table 2-2. Prestressing Data Summary

Avg. Values	Hoop	Vertical
Design Tension Forces	44.4 Tonnes (97.9 K)	49.6 Tonnes (109.3 K)
Jack Force	43.6 Tonnes (96.1 K)	49.0 Tonnes (108.1 K)
Design Lift-off Force	34.1 Tonnes (75.2 K)	46.3 Tonnes (102.1 K)
Jack Lift-off Force	34.0 Tonnes (75.0 K)	44.2 Tonnes (97.5 K)
Load Cell Force (5/4/00)	33.3 Tonnes (73.52 K)	43.6 Tonnes (96.04 K)
Load Cell Force (7/6/00)	33.1 Tonnes (73.04 K)	43.5 Tonnes (95.85 K)
Friction Coeff.	0.18	0.22
Seating Loss (mm)	3.95 mm	4.95 mm
Seating Lost Force	9.56 Tonnes (21.09 K)	4.79 Tonnes (10.56 K)

2.2.2.1 Axisymmetric Analysis
After extensive review of the data, it was decided to use the average load cell force recorded approximately two months after completion of prestressing, on July 6, in the axisymmetric analysis. This includes stress redistributions due to tendon relaxation, seating, and initial effects of creep. Judging by the very limited change from May to July, the July value appears to be a very stable value and it is apparent that creep effects may have been much smaller than anticipated, or partially offset by change in ambient thermal conditions between May and August.

The measured friction coefficients for the hoop and vertical tendons (0.18 and 0.22) were close to the design value assumed prior to the test (0.21). However, there is a great deal of conflicting information in reaching these final friction coefficient conclusions. For example, the measurements for the instrumented vertical tendons show that angular friction may be greatly overstated, but setting losses and "wobble" friction may be understated. The reverse may be true for the hoop tendons. The hoop tendon friction is discussed in more detail for the 3DCM. Since there is no hard-and-fast conclusion on the friction coefficient, it was decided to stay with angular friction that is based on NUPEC's original measurements, namely $\mu = 0.21$ for the hoop tendons. For the vertical tendons, some changes were adopted.

The hoop prestress values relevant to the axisymmetric analysis were recomputed as follows:

Hoop Tendons
The azimuth at which 3.95 mm loss is absorbed/balanced by tendon friction = 39.5° from buttress centerline (by separate calculation; see 3DCM discussion)

$$T_2 = T_1 \ e^{-\mu \propto} \qquad (\mu = 0.21)$$

Stress at load cell = 73.04 K/.525 in² = 0.96 MPa (139.1 ksi)

Stress at anchor set balance/absorption point = 1.074 MPa (155.7 ksi)

The stresses at the 135° azimuth were recalculated as:

$$s_{Group1} = 155.7e^{-\left(.21x955x\frac{\Pi}{180}\right)} = 109.7 \; ksi \quad \left(757 \; MPa\right)$$

$$s_{Group2} = 155.7e^{-\left(.21x5.5x\frac{\Pi}{180}\right)} = 152.6 \; ksi \quad \left(1052 \; MPa\right)$$

These hoop prestress values are 5% lower than those used in the earlier analysis.

Vertical Tendons
The strain gage measurements on V46 and V37 (plots attached as Figure 2-2 and 2-3) show much different stress distributions than originally assumed. The axisymmetric model was not originally set up to model vertical tendon anchor set or wobble friction. However, judging by the measurements of Tendon V46, some simulation of stress variation along the straight vertical tendon segments was needed. From Table 2-2, the average force measured in the vertical tendons on July 6, 2000 was 43.47T (95.85k). For Tendon 46, it was 42.18T (93 kips), and there were significant losses along the cylinder barrel section of the model (see Figure 2-2). Without having much additional data, Tendon V46 was used as a prototype for the final axisymmetric analysis vertical tendon stress distribution. As such, the anchor force was set equal to 42.18T (93 kips). The stress at the anchor is therefore

$$\sigma_{vertical} = 42.18T/3.393cm^2 = 1222 \; MPa \; (177 \; ksi).$$

A friction tie strategy similar to the dome strategy of the earlier axisymmetric models was adopted and implemented as shown in Figures 2-4, 2-5, and 2-6. The resulting stress distribution after prestressing and equilibration is shown in Figure 2-7. The stress results are also shown on the measurement plots in Figures 2-2 and 2-3. The anchor force used is about 8% less than that for the prior pretest analysis. For friction, an angle for the 5 friction ties of 11.70 degrees was selected to achieve the stress losses shown in the figures. This friction tie modeling strategy was explained in detail in the pretest analysis report [1].

2.2.2.2 3DCM Model
The 3DCM model behavior was found to be sensitive to the extent of anchor set; thus more discussion is warranted for making the final tendon stress assumptions for this model.

The 3DCM model spans vertically from hoop tendon H35 to H72. The prestressing tendon tensioning data [1] shows that the average hoop tendon seating loss is 3.95 mm when averaged over all hoop tendons *and* when averaged over H35 to H72. Therefore, it was decided to use 3.95 mm for the seating loss on all hoop tendons. This put the seating loss zone of influence at 39.5 degrees from the buttress centerline, which creates a case that is partway between Case 1 and Case 2 from the early 3DCM anchor set loss sensitivity study [1]. This assumption appears to agree fairly well with the strain gage data points on the hoop tendons that were instrumented (H35, H53, and H68) (see Figures 2-8 to 2-13). The measured strains/forces at the midpoints of H53 and H68 imply that the angular friction may be a little smaller than the design value (0.18 versus 0.21), but the H35 measurements show that near penetrations where the tendon path curves around the penetrations, the effective angular friction may be higher than the design value. For the tendons represented in the 3DCM, it was assumed that the design value 0.21 (as measured by NUPEC in separate mock-up tests) would provide a reasonable average of the varying conditions that occur in the cylinder-midheight region. Note that the initial stress profile of H35 simulated in the 3DCM mimics the plotted measurements, with the minimum stress position at a point closer to the equipment hatch, rather than at the tendon midpoint (90 degrees). This is because of the extra local angle changes that the tendon passes through when sweeping around the E/H.

Although it would be possible to input different hoop tendon stresses in each tendon, it was decided to use the average load cell value of 32.89T (72.5 kips) that existed at the July 6 measurement. The load cell measurements for H40 (End A) and H58 (End A) appear unreasonably low compared to the jacking forces, and an average force seems more appropriate. The target hoop prestress at the anchors, therefore, was

$$s_{anchor} = \frac{32.89T}{3.393cm^2} = 952MPa\left(138.1ksi\right).$$

The final hoop tendon stress profiles produced are shown in Figures 2-8 through 2-16.

2.2.3 Creep, Temperature, and Other Time Dependent Effects

Judging by the minimal change in the tendon forces between May and July, the effects of creep and shrinkage appear to be much smaller than anticipated. It is difficult, however, to isolate the creep response from other time-dependent effects, such as temperature. Since creep effects will tend to be largest within the first 30 to 60 days after prestressing, using the July 6 measured prestress values accounts for time-dependent effects reasonably well. In general, as is shown in Figures 2-8 to 2-13, the initial levels of prestress arrived at are lower than those measured on individual tendons by between 3% and 10%. This should accommodate creep effects that may occur between July 6 and September 26, but no further creep and temperature effect simulations have been performed other than the one discussed in the pretest analysis report [1].

2.3 Data Presentation

The goals of the final pretest prediction analysis were to update the prediction results with analyses that included the latest material properties and tendon stress conditions. As noted, this was done primarily to support test operations by providing the 'best' predictions of the model's response for real-time comparison to the actual response. The following suites of data were provided for making real-time comparisons during the test:

1. All Standard Output Locations (SOL);

2. Four sets of displacement profile data versus pressure (vertical sections at 90 degrees, 135 degrees, and 324 degrees and a horizontal profile at Elev. 4.7m);

3. Four sets of strain data to be displayed on panels (E/H, A/L, M/S and Wall-Base Juncture).

Some of the more important plots with the published and final pretest predictions are presented in Chapter 4. The radial displacements at the bottom and top of the final 3DCM model are compared to the final axisymmetric model results in Figures 2-17 and 2-18. Comparing to the previous pretest analysis shows a trend of slight reduction in 3DCM radial displacement and an increase in axisymmetric radial displacements. This brings the 3DCM radial displacement results, at 135 degrees, a little closer to the axisymmetric results, but there is still a substantial difference between the two. Developing a final suite of analysis data to compare to test data during the test meant choosing between cylinder radial displacement data predicted by the two different models. To this end, it was decided to use a spatial interpolation scheme to develop a consistent set of displacement data for the entire cylinder. The difference between the 3DCM model and axisymmetric model radial displacements is one of several posttest evaluation topics in this report.

2.4 Conclusions of Final Pretest Analysis

Final changes to the pretest prediction analyses were documented prior to the test and summary results. Based on the final analyses, the general failure mode prediction, liner tearing near the equipment hatch, did not change; nor did the failure (leakage) pressure, 3.2 Pd. The final ranking and predicted sequence of failure locations was previously published in the pretest predictions report [1]. Those predictions are repeated below for reference.

Table 2-3. Possible Liner Tearing Locations in Descending Order of Probability of Occurrence

Most Likely Occurrence	Location
1.	E/H near vertical T-anchor termination (4 locations, Type 3);
2.	E/H near horizontal stiffener termination(4 locations, Type 2);
3.	Near a weld seam with hoop stiffener rat-hole, 5 degrees from the centerline of 90 degree buttress (i.e. 95 degrees; occurs in roughly 6 locations);
4 and 5	Similar to 1 and 2, but near the A/L (7 locations, Types 3 and 2);
6.	Similar to 1, but near the M/S penetration (2 locations, Type 3);
7.	Similar to 1 and 2, but near the feedwater (F/W) penetration (3 locations, Types 3 and 2);
8.	Strain concentration Location Type 4 near F/W penetrations, M/S penetrations.
9.	Liner tear at wall-basemat juncture.

D3

D2

D1

	Concrete Pour	Specified Strength
	Completion Date	F'c (MPa)
F1	2-12-97	29.42
F2	2-28-97	29.42
F3$_A$	5- 8-97	29.42
F3$_B$	5- 8-97	44.13
F4	7- 2-97	44.13
	Pour Date	F'c (MPa)
C1	11-11-98	44.13
C2	12-10-98	44.13
C3	1-5-99	44.13
C4	1-28-99	44.13
D1	3-3-99	44.13
D2	4-12-99	44.13
D3	4-15-99	44.13
F5	5-24-00	29.42
F6	6-9-00	44.13

C4

C3

All C1 average

C2

C1

F4

F3$_A$

F3$_B$

F2

F6

F3B average

F1

Rest of Basemat
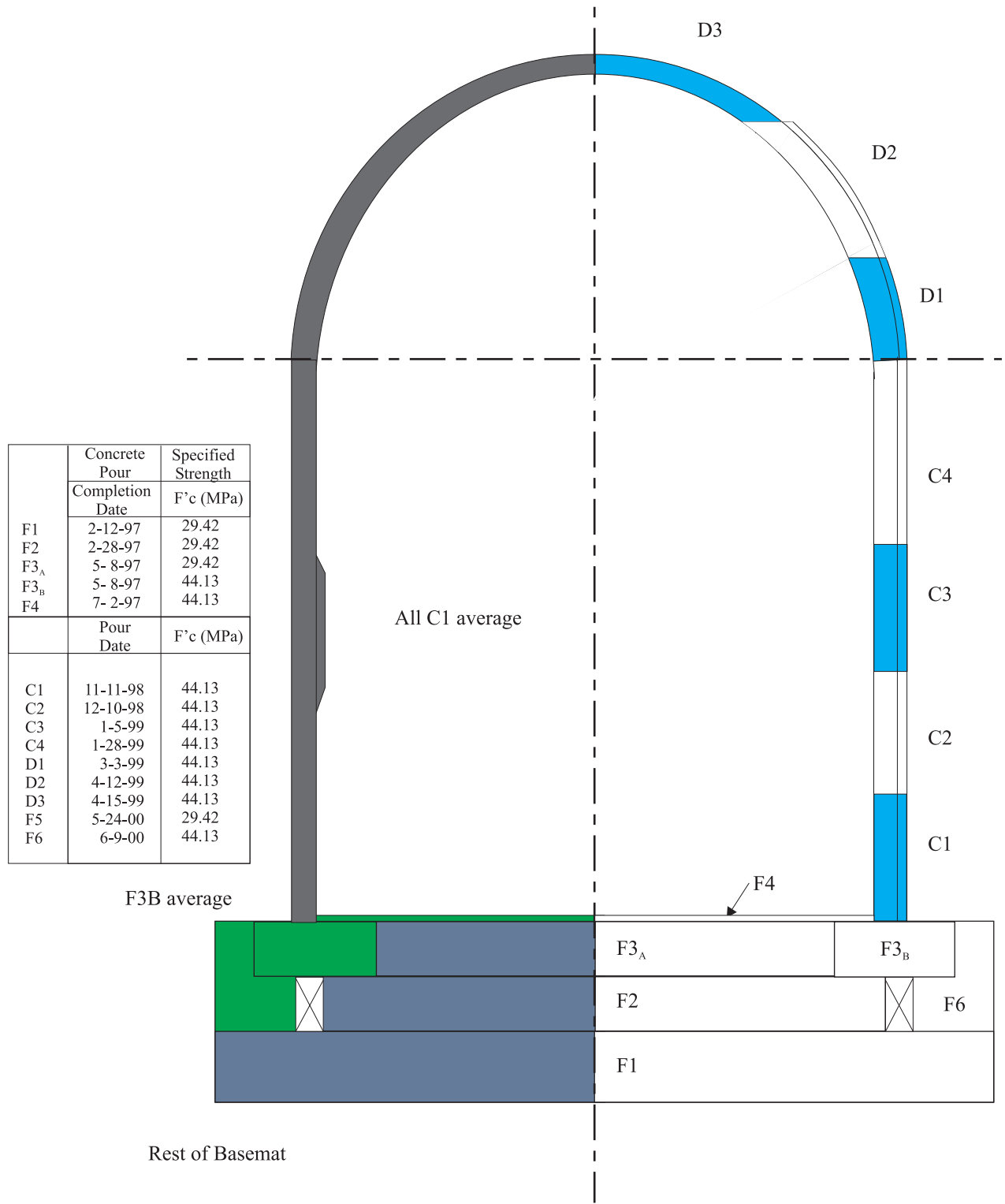
Figure 2-1. PCCV Model with Revised Concrete Pour Schedule
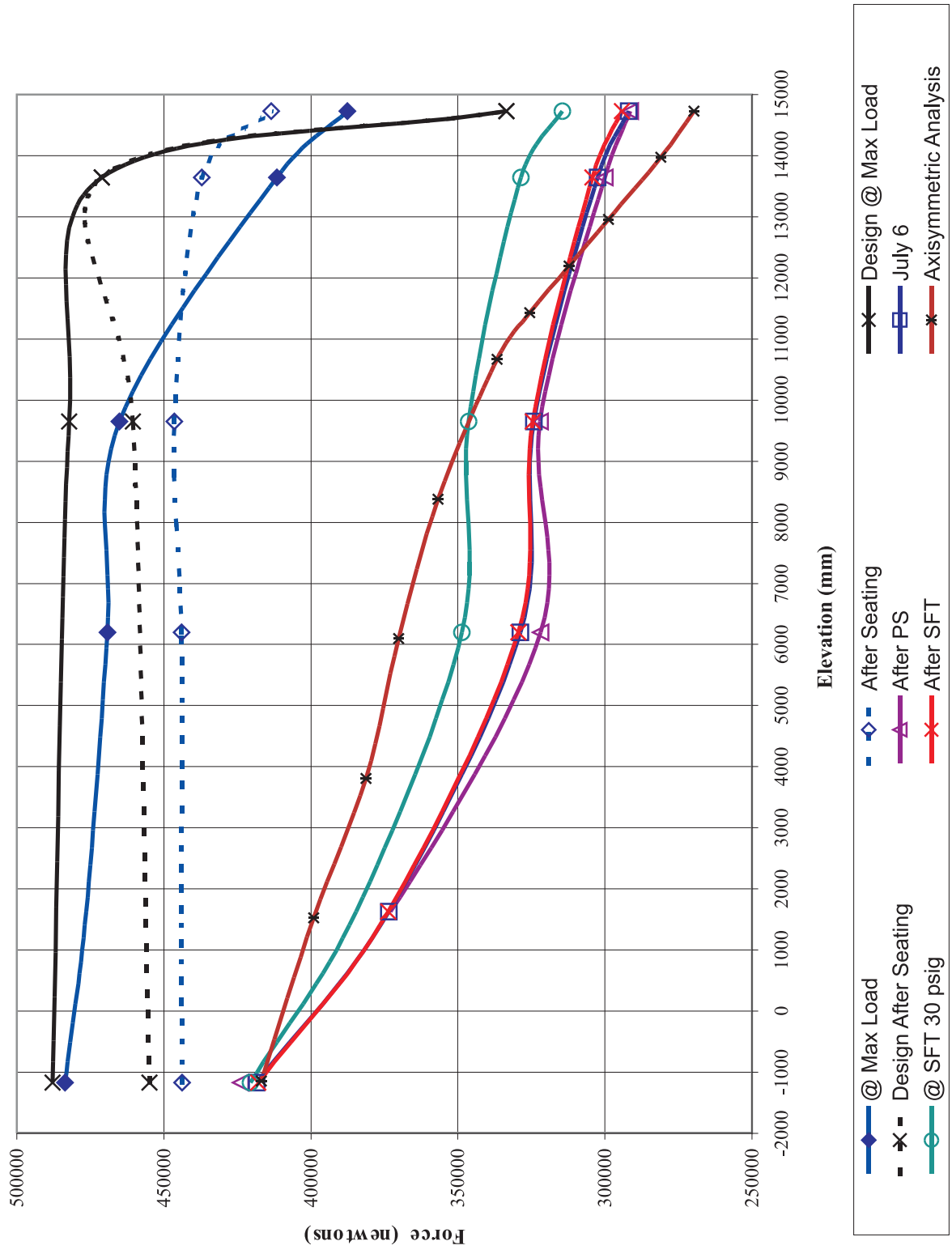
Figure 2-2. Tendon Force Measurements for Vertical Tendon #V46
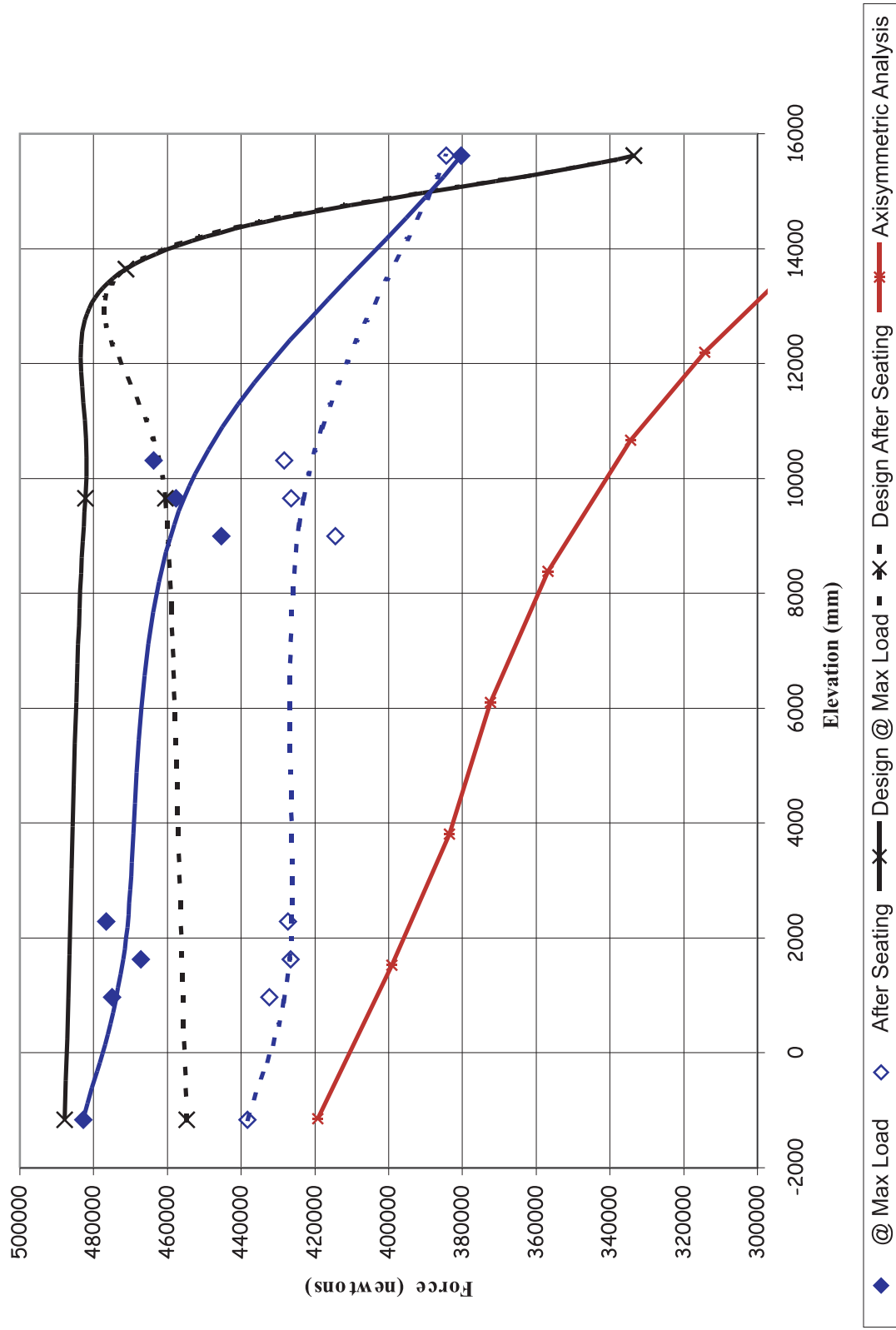
Figure 2-3. Tendon Force Measurements for Vertical Tendon #V37

Tendon

Top of
Cylinder

Symmetry Line
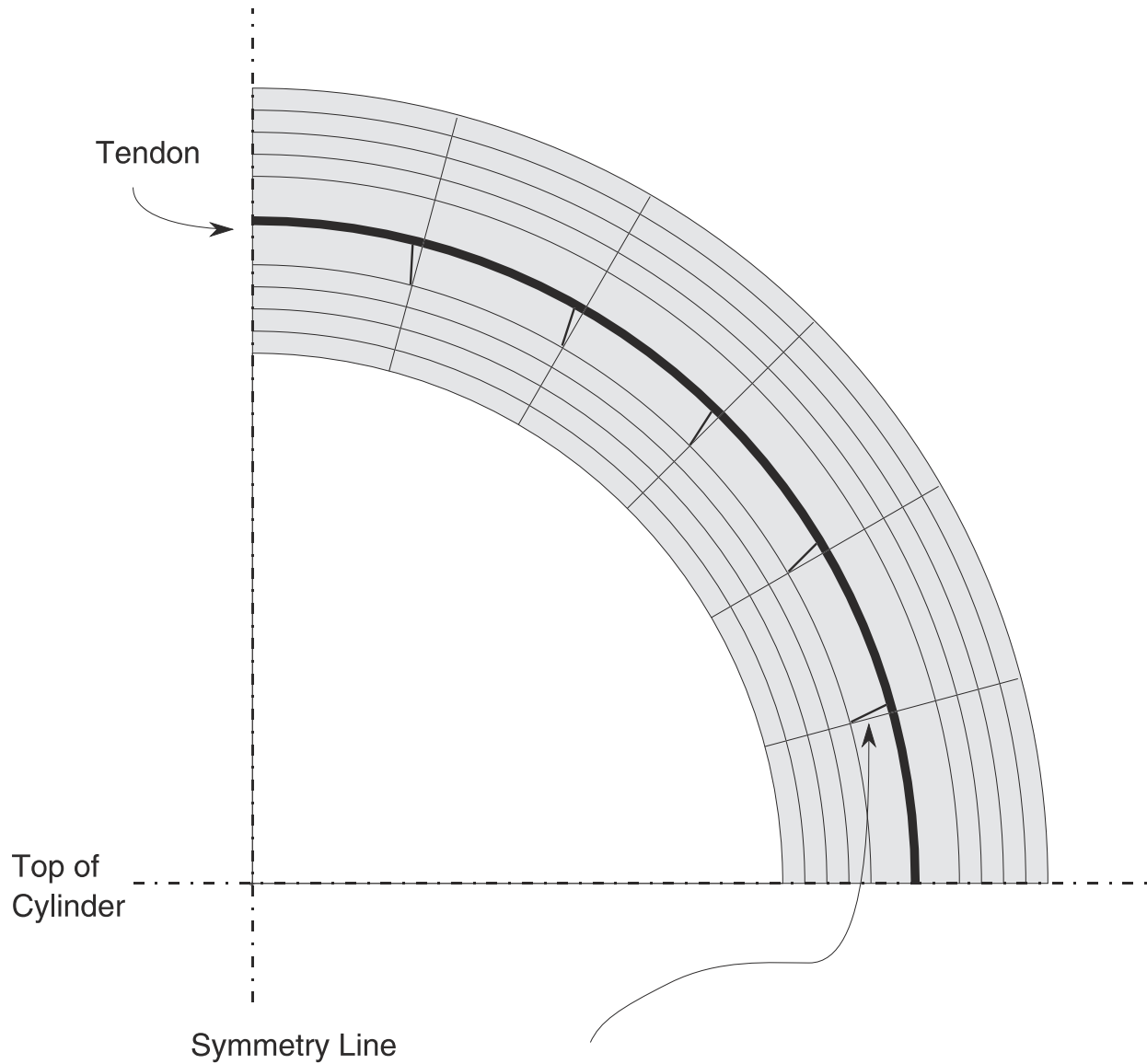
(Not to Scale)

Friction Trusses at All Nodes
Between Vertical Dome Tendon and Concrete

Friction Angle, $\alpha = $ Arctan(μ)
(Angle from Radial Projection to Truss)

where $\mu = 0.21$

Length of Friction Truss = $\dfrac{\text{Radius of Tendon Duct}}{\cos(\alpha)}$

Figure 2-4. Modeling of Tendon Friction Behavior

(Not to Scale - Actual Element Density Not Shown)

Position of Nodes Moved to Add Friction

Vertical Tendon (Connected to Concrete Nodes by Truss Elements)

Prestressing Gallery

Mathematical Constraints from End of Jacking Element to Tie-Down Nodes

Jacking Force

Extra Element to Apply Prestressing Strain
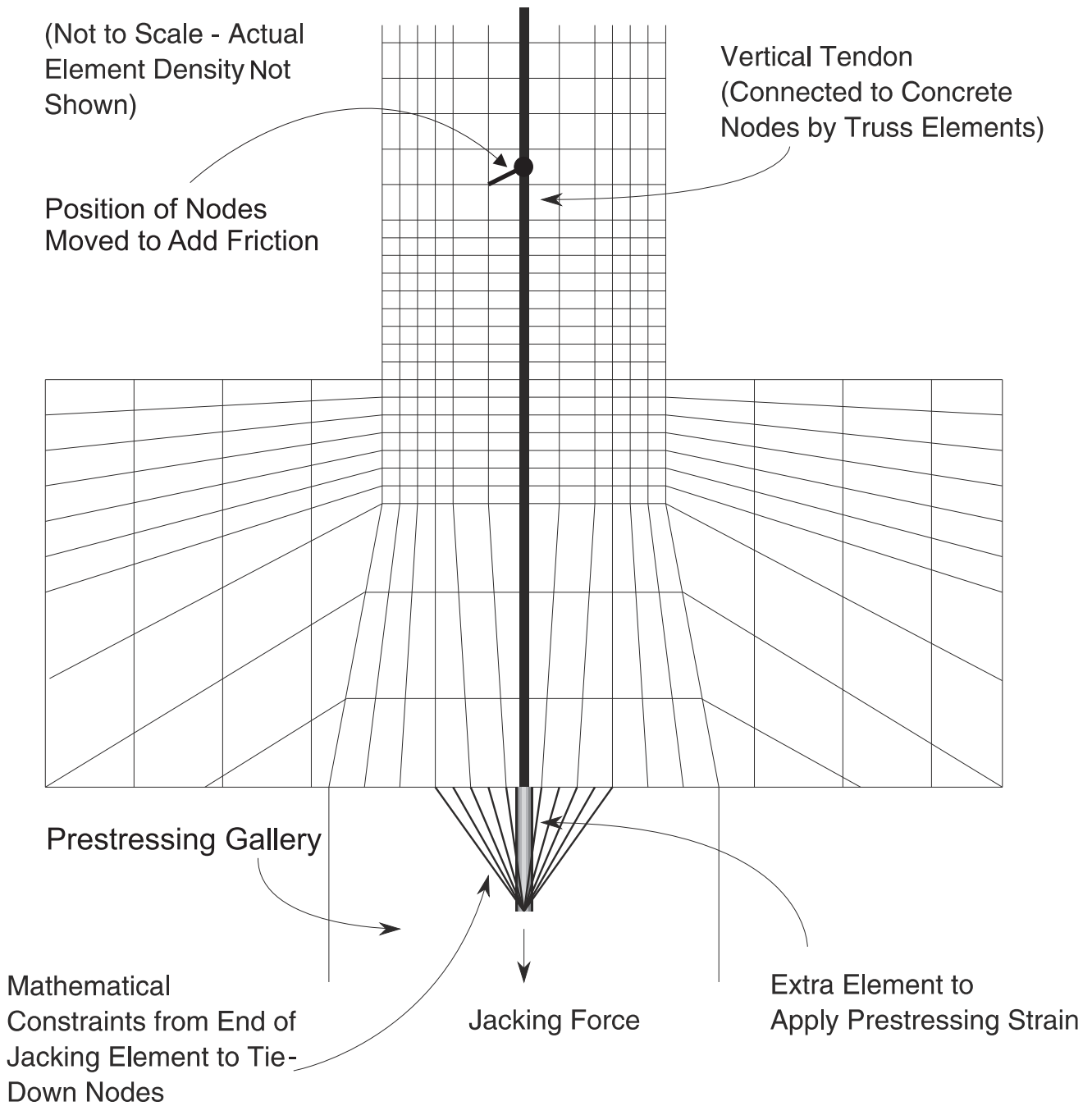
Jacking Force is Applied as an Initial Stress in the Jacking Element.

Figure 2-5. Modeling of Prestress Application with Jacking Element

5

4
(45° Dome Angle)

Locations of Five
Added Friction Ties

3

2

1

Basemat

Nonlinear Springs at Base
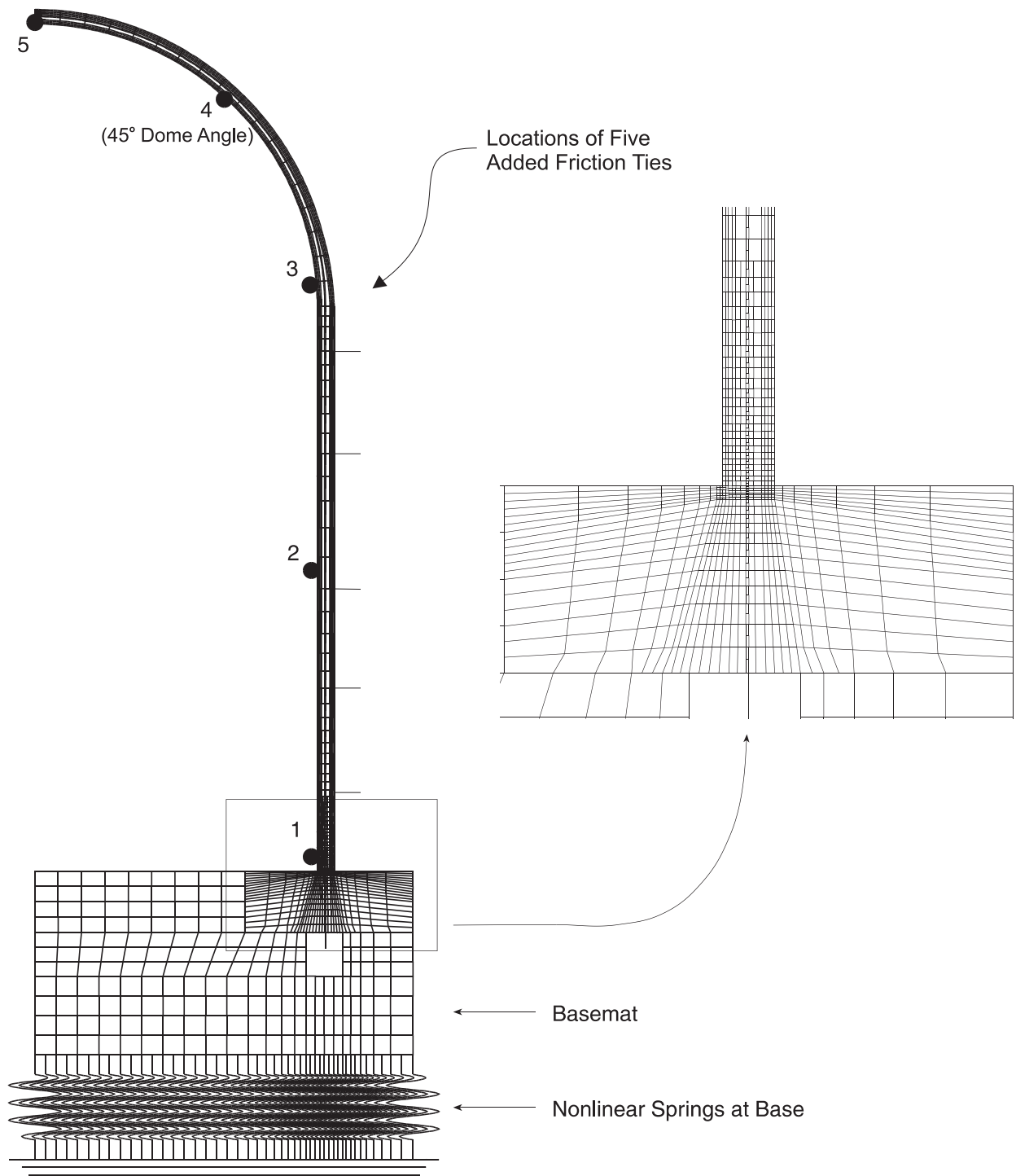
Figure 2-6. Axisymmetric Model of PCCV and Locations for Plotted Output

SECTION POINT 1

S11   VALUE
+7.86E+02
+8.30E+02
+8.73E+02
+9.16E+02
+9.59E+02
+1.00E+03
+1.05E+03
+1.09E+03
+1.13E+03
+1.18E+03
+1.22E+03

C SCALE= 6.89E-3

Top of Basemat;
Elevation, 0 mm

Elevation, -1175 mm
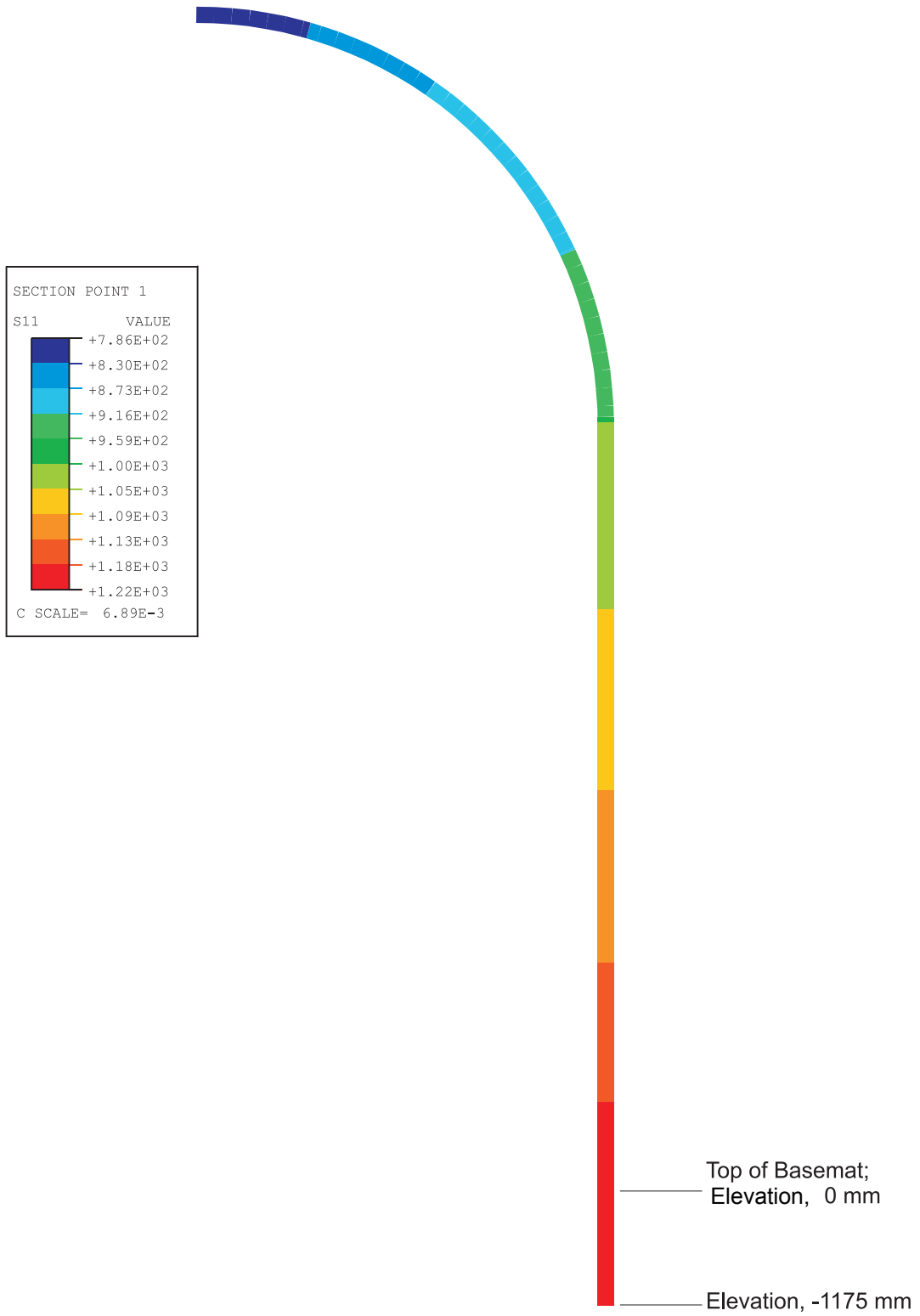
Figure 2-7. Vertical Stress (MPa) in Vertical Tendons after Prestress

23
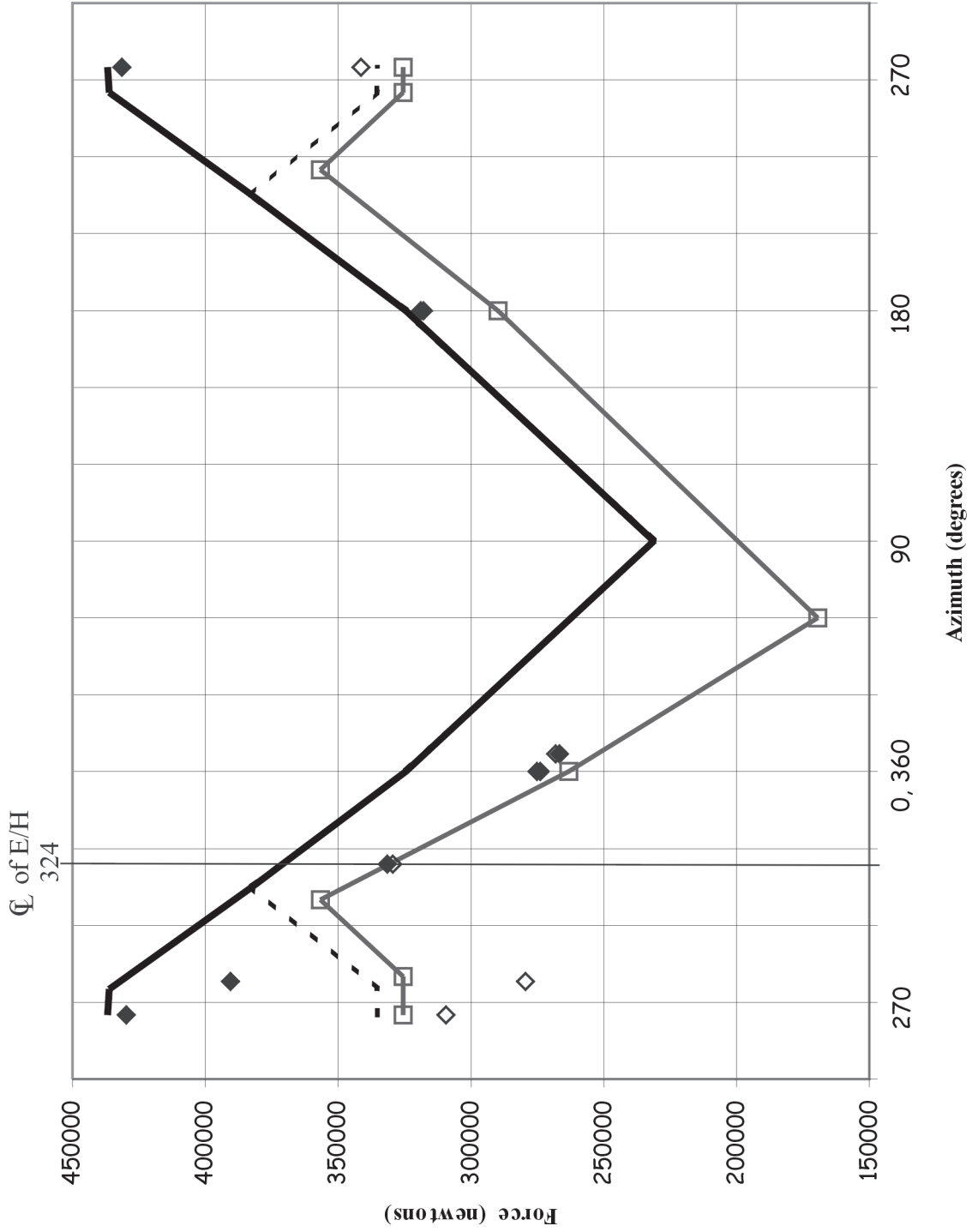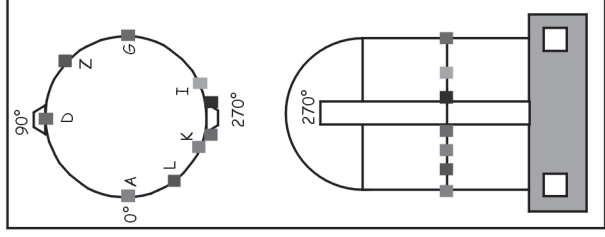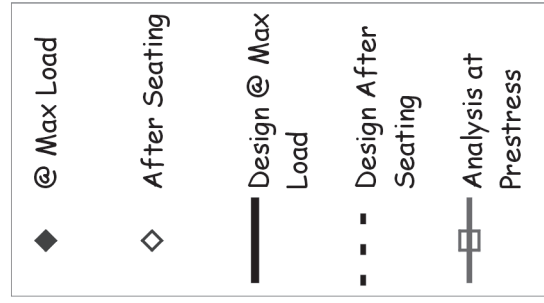
Figure 2-8. Tendon H35 Force Distribution (Strain Gage Data)
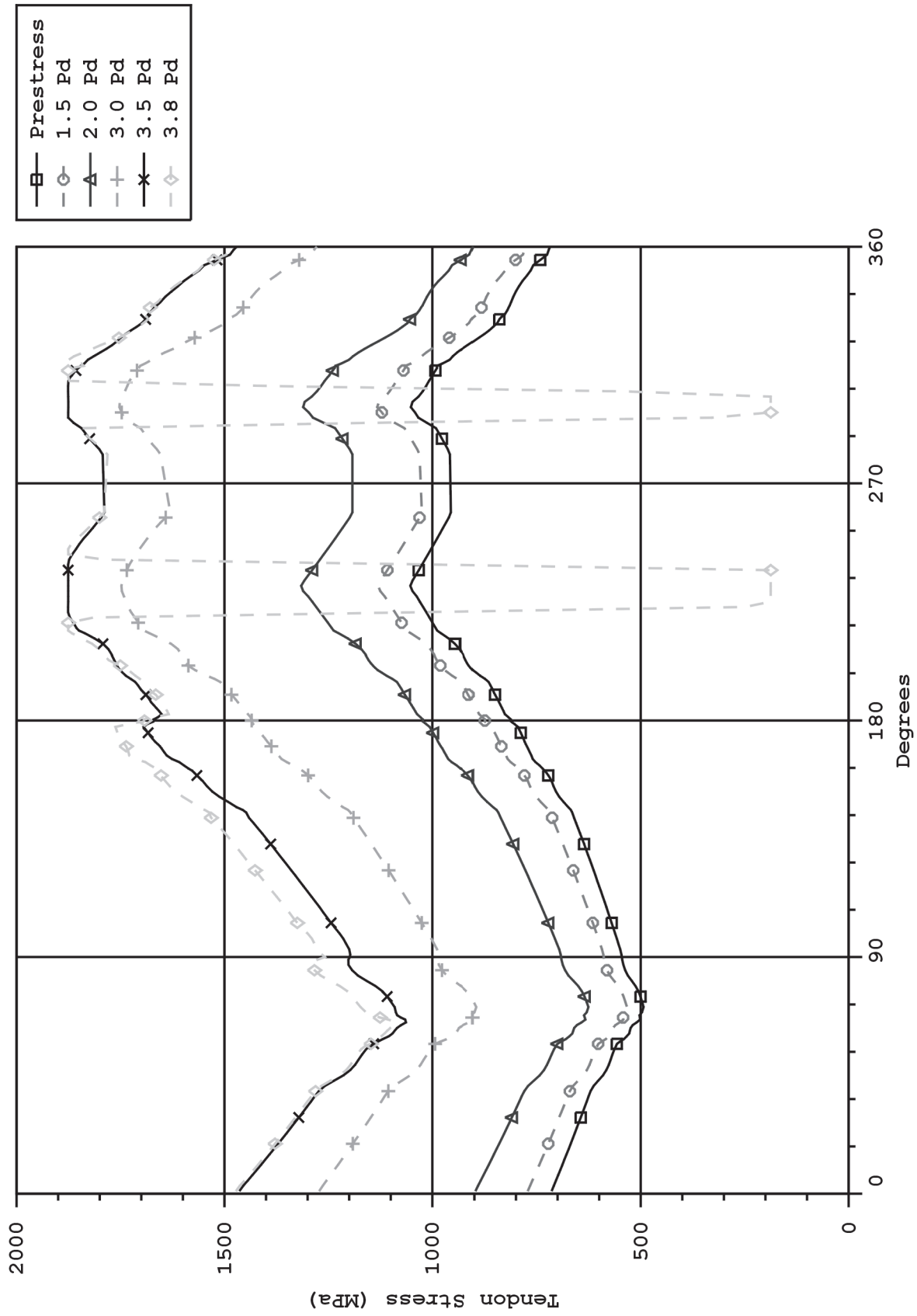
Figure 2-9. Tendon Stress Profile for Instrumented Hoop Tendon #H35
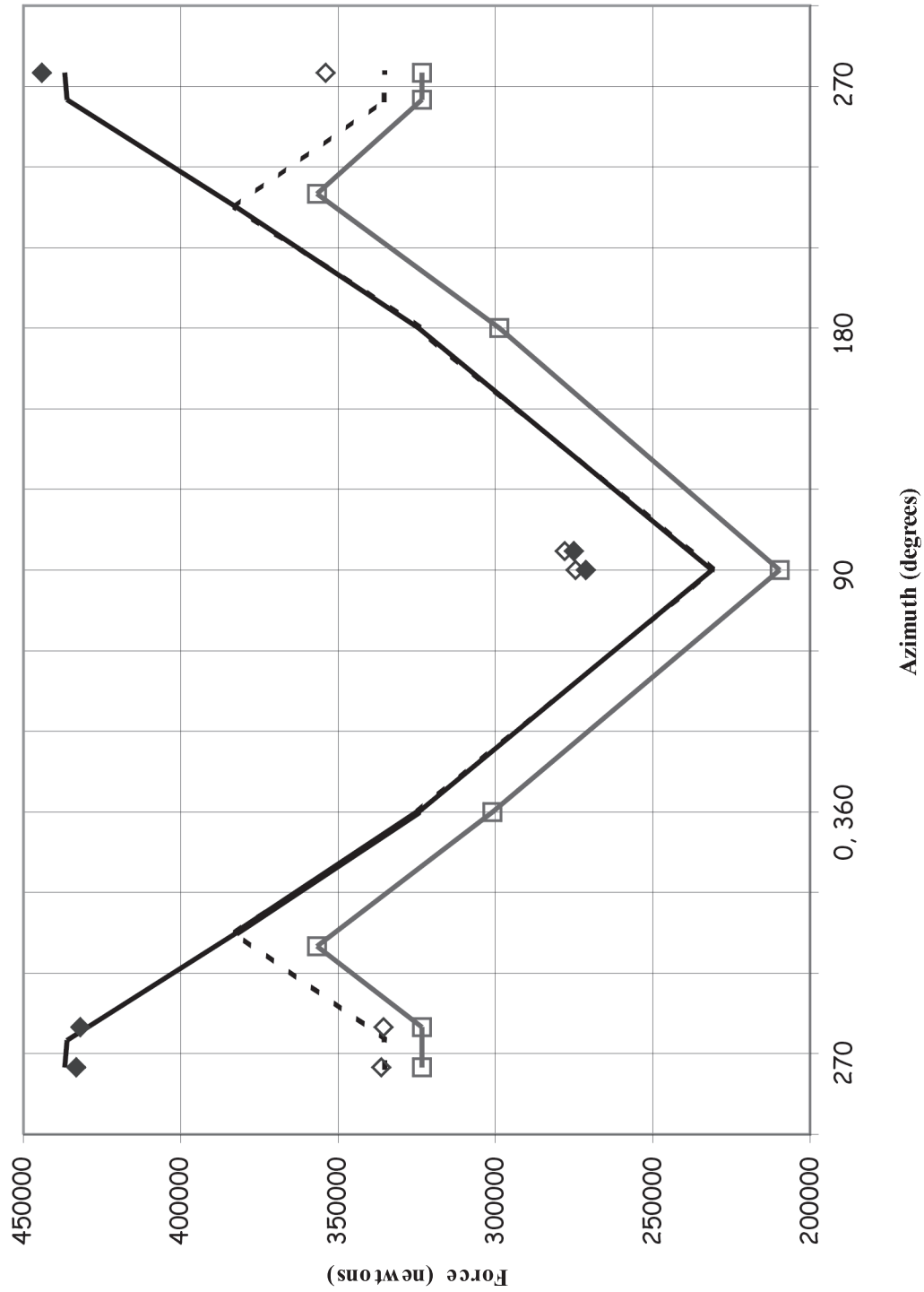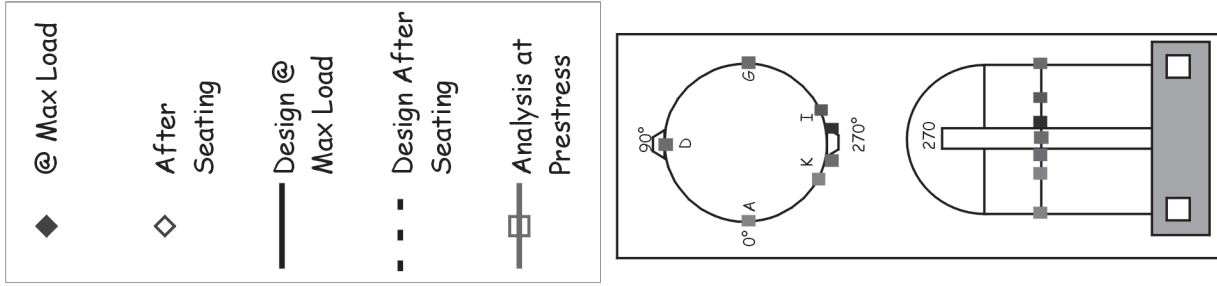
Figure 2-10. Tendon H53 Force Distribution (Strain Gage Data)
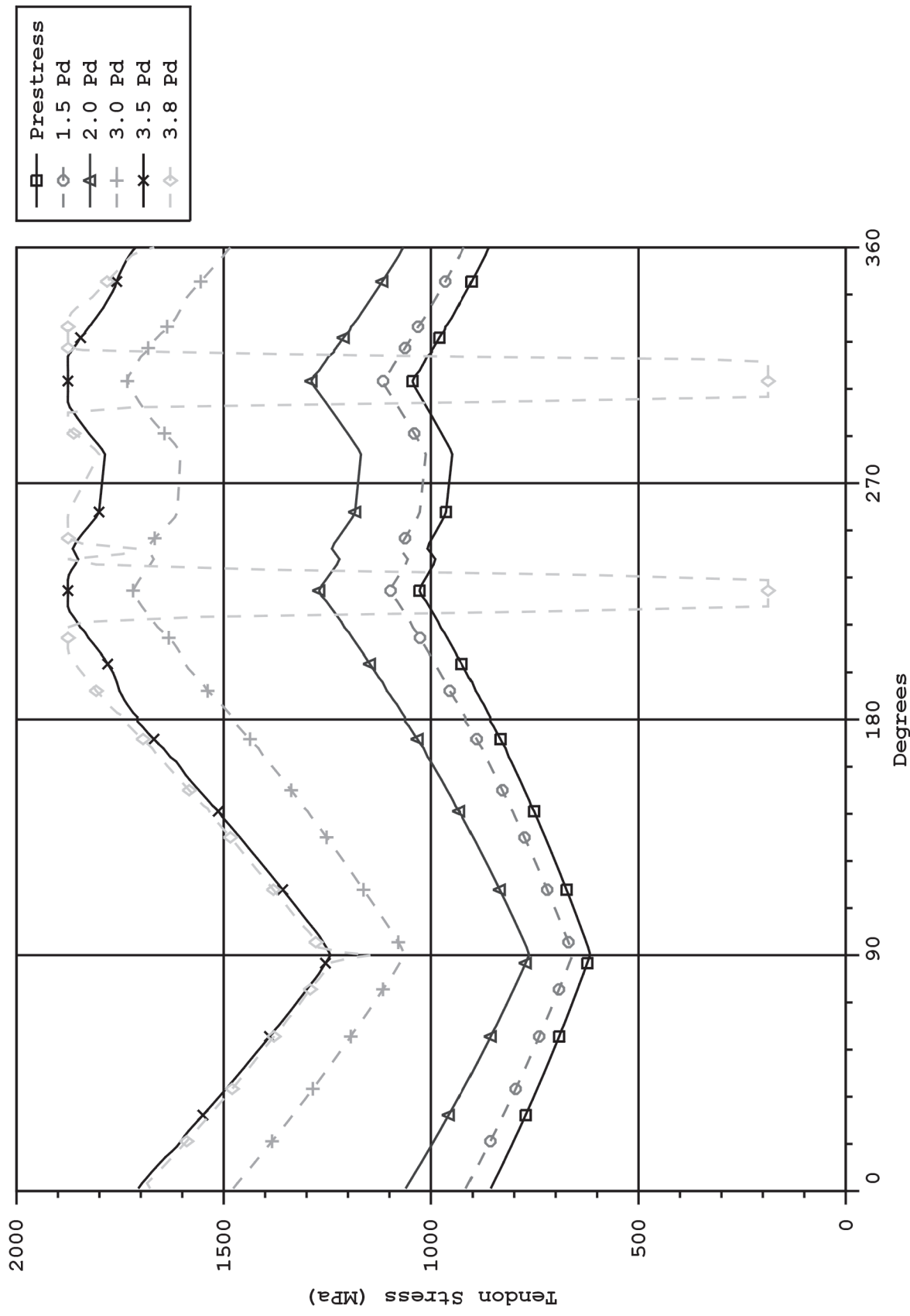
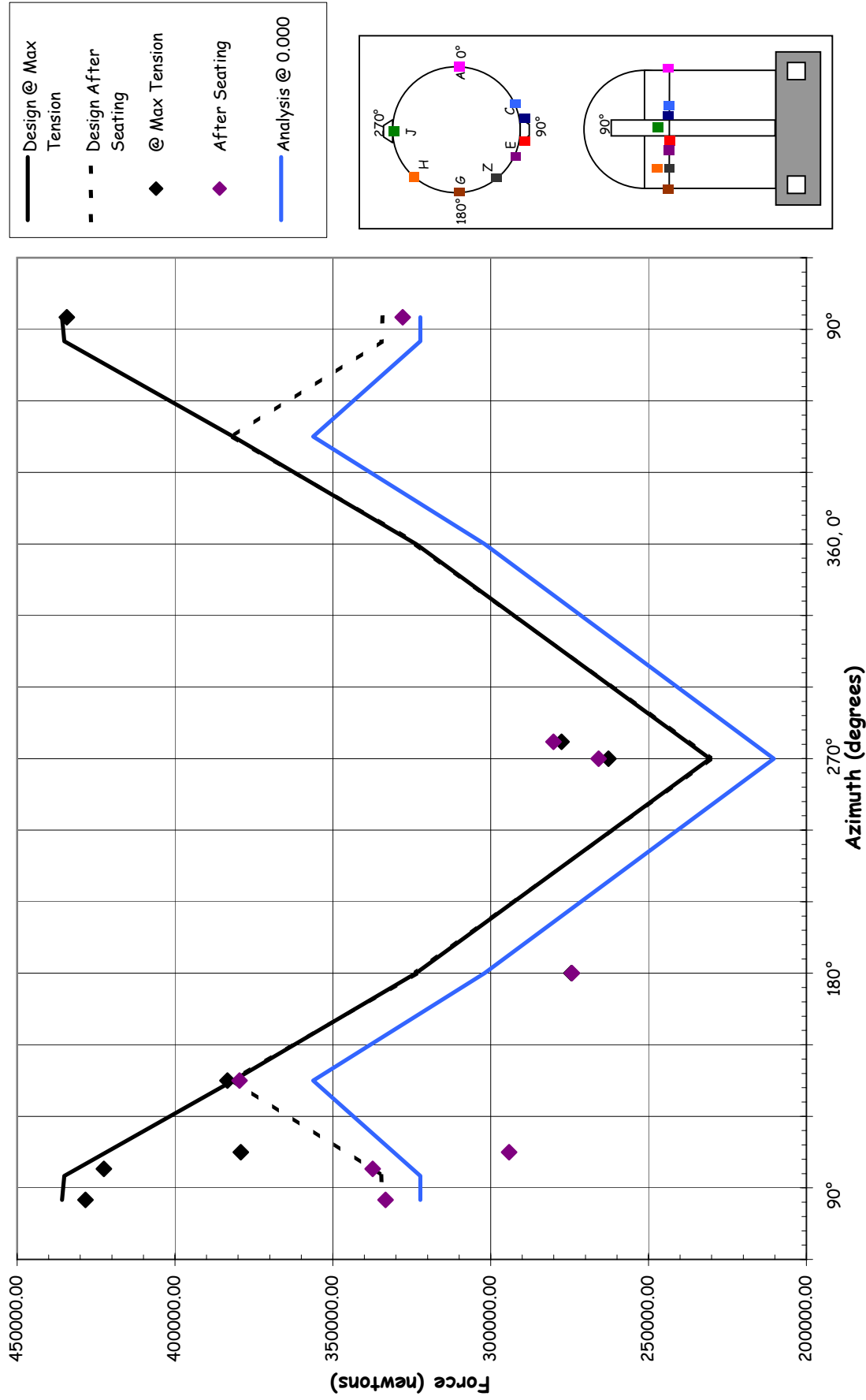Figure 2-11. Tendon Stress Profile for Instrumented Hoop Tendon #H53

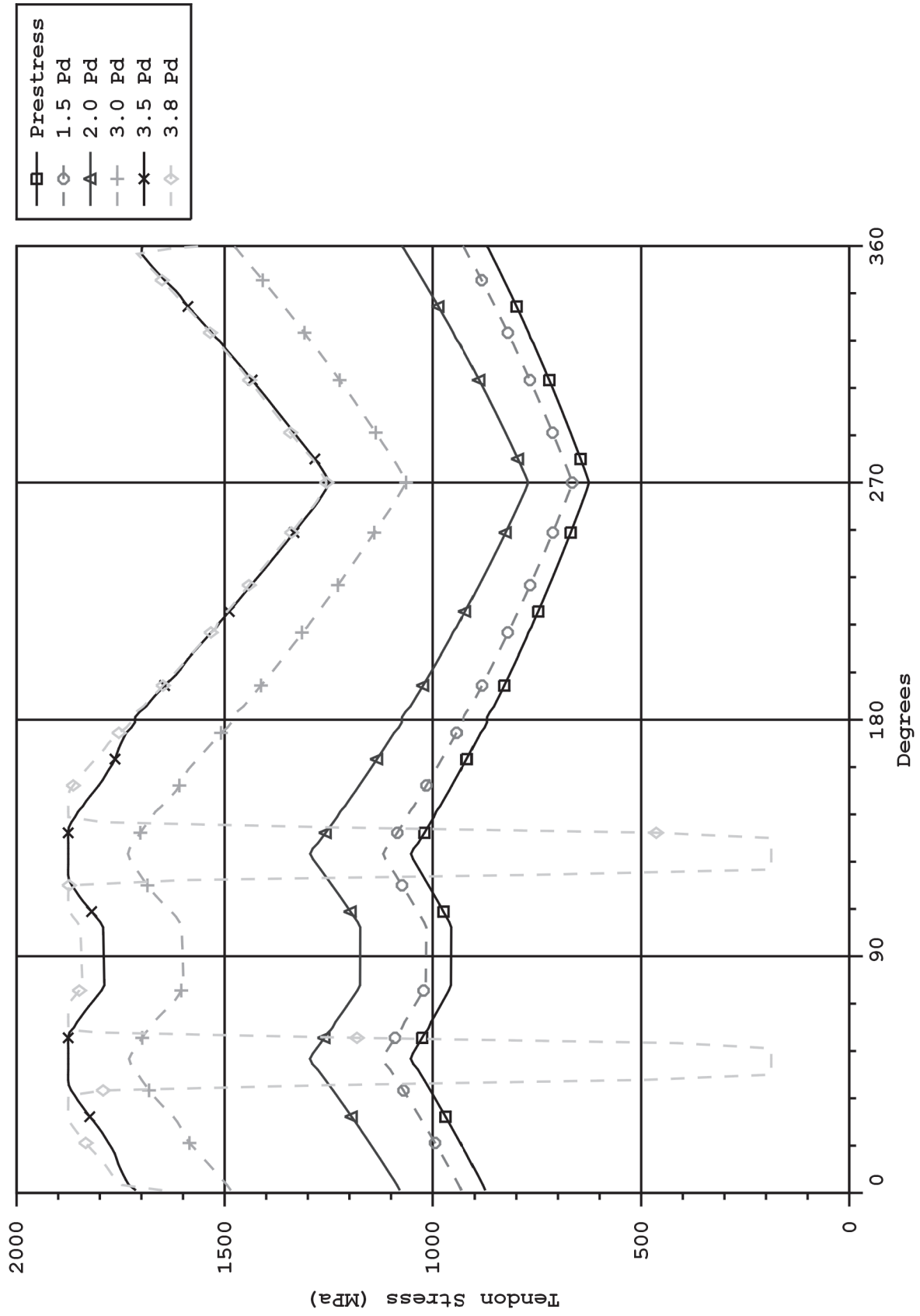Figure 2-12. Tendon H68 Force Distribution (Strain Gage Data)

28

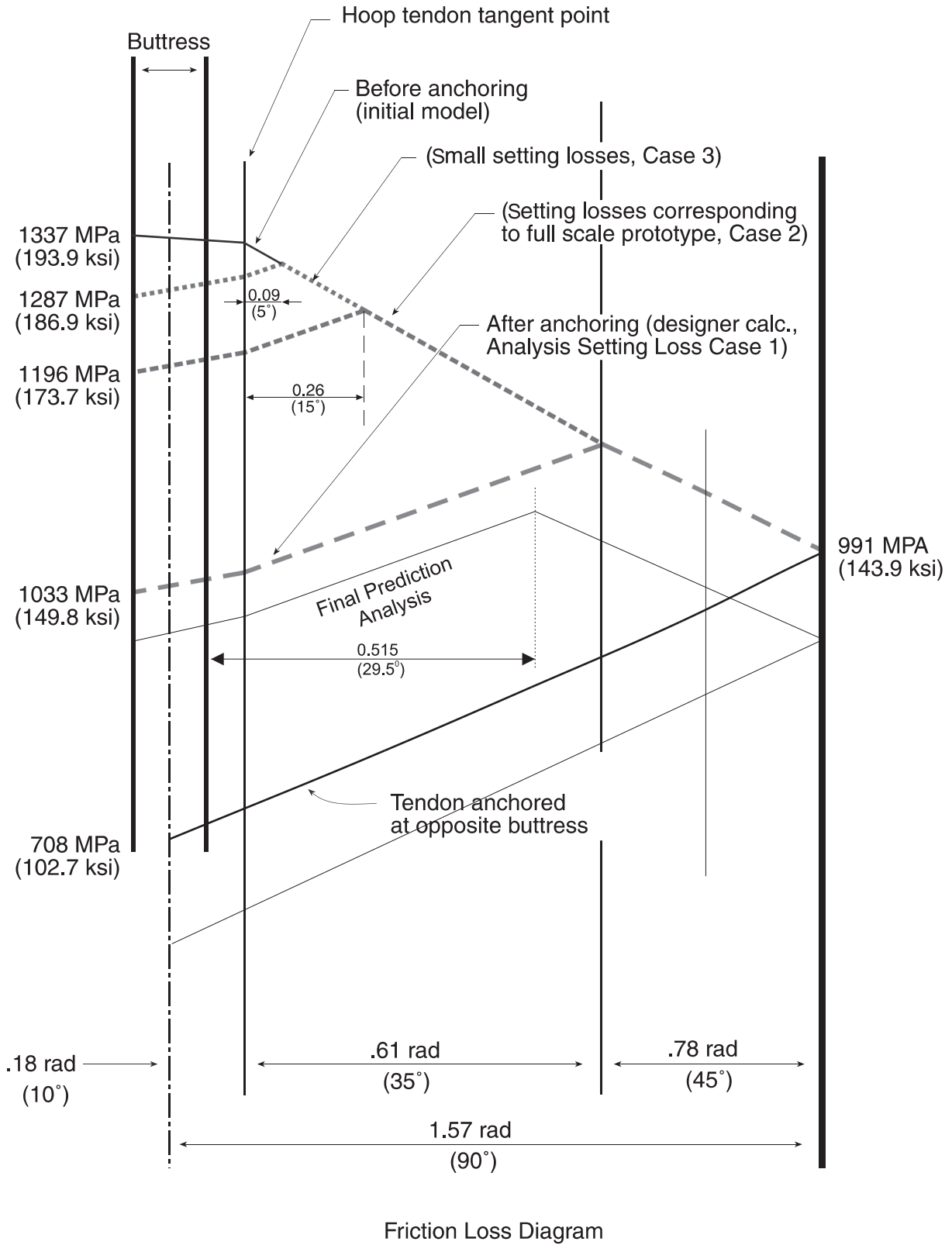Figure 2-13. Tendon Stress Profile for Instrumented Hoop Tendon #H68

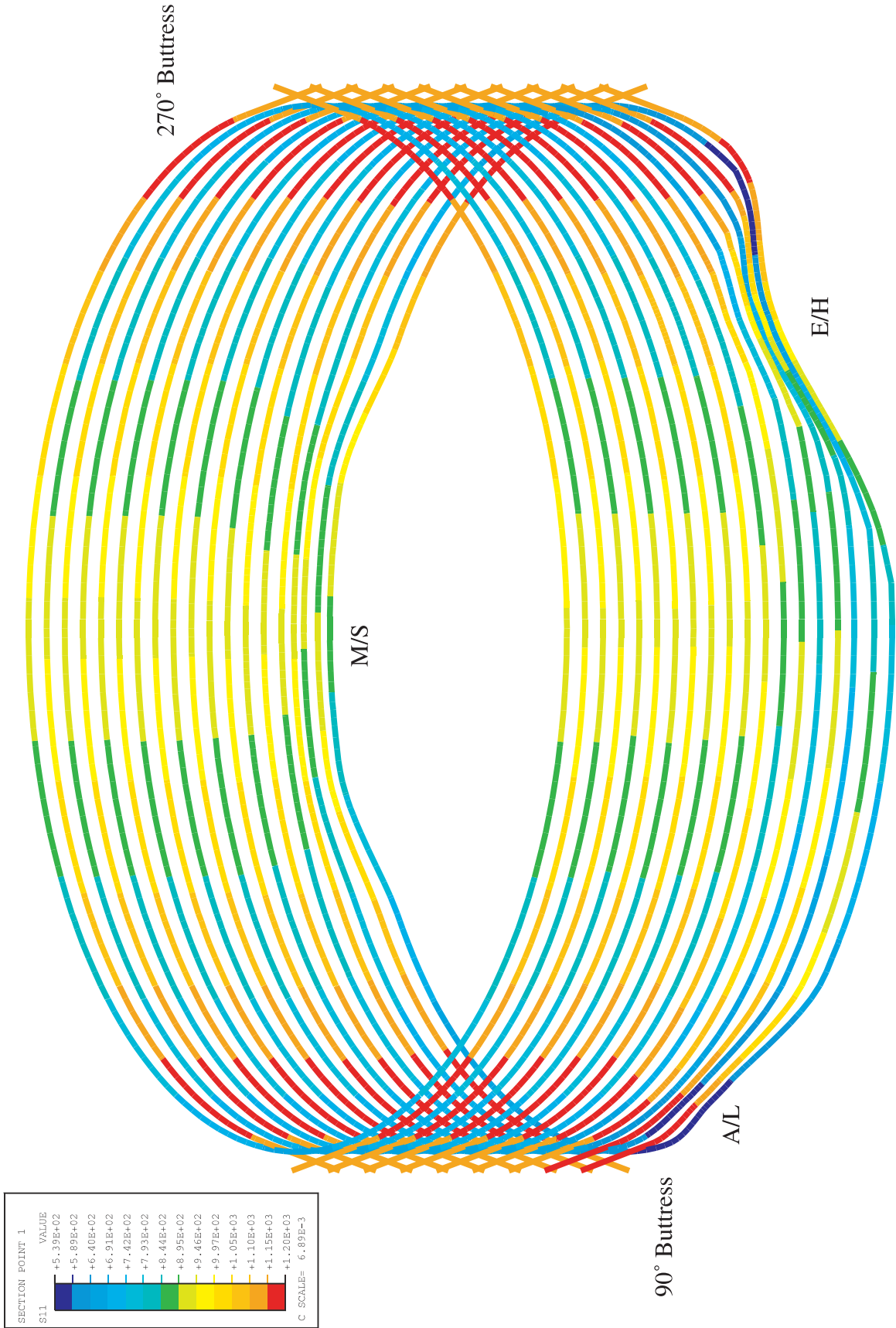Figure 2-14. Other Setting Loss Cases for Parameter Study

30

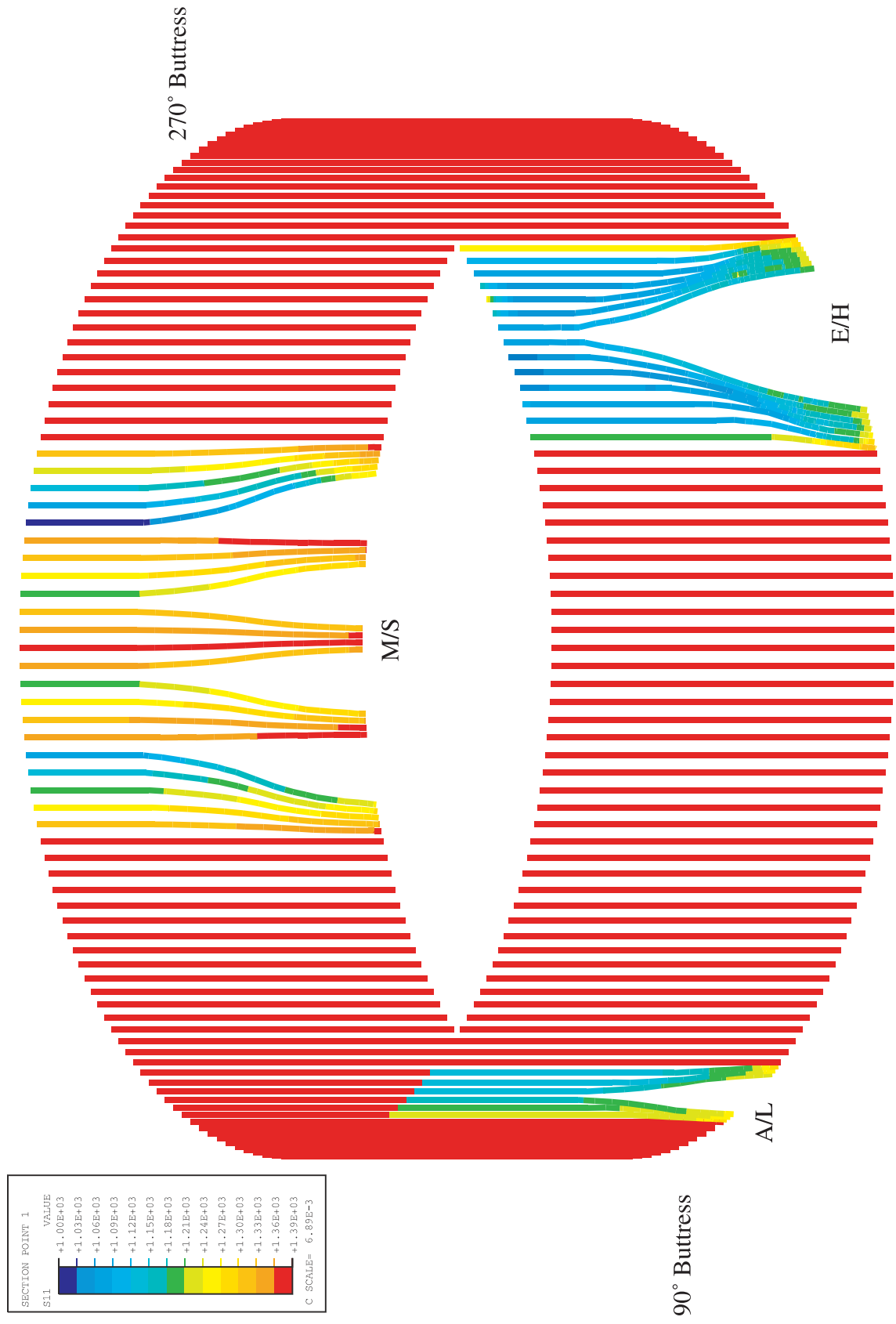Figure 2-15. Stress Contours (MPa) in Hoop Tendons After Prestress

270° Buttress

E/H

M/S

90° Buttress

A/L

SECTION POINT 1
S11   VALUE
      +5.39E+02
      +5.89E+02
      +6.40E+02
      +6.91E+02
      +7.42E+02
      +7.93E+02
      +8.44E+02
      +8.95E+02
      +9.46E+02
      +9.97E+02
      +1.05E+03
      +1.10E+03
      +1.15E+03
      +1.20E+03
C SCALE= 6.89E-3

31

Figure 2-16. Stress Contours (MPa) in Meridional Tendons after Prestress

270° Buttress

E/H

M/S

A/L

90° Buttress

SECTION POINT 1
S11   VALUE
    +1.00E+03
    +1.03E+03
    +1.06E+03
    +1.09E+03
    +1.12E+03
    +1.15E+03
    +1.18E+03
    +1.21E+03
    +1.24E+03
    +1.27E+03
    +1.30E+03
    +1.33E+03
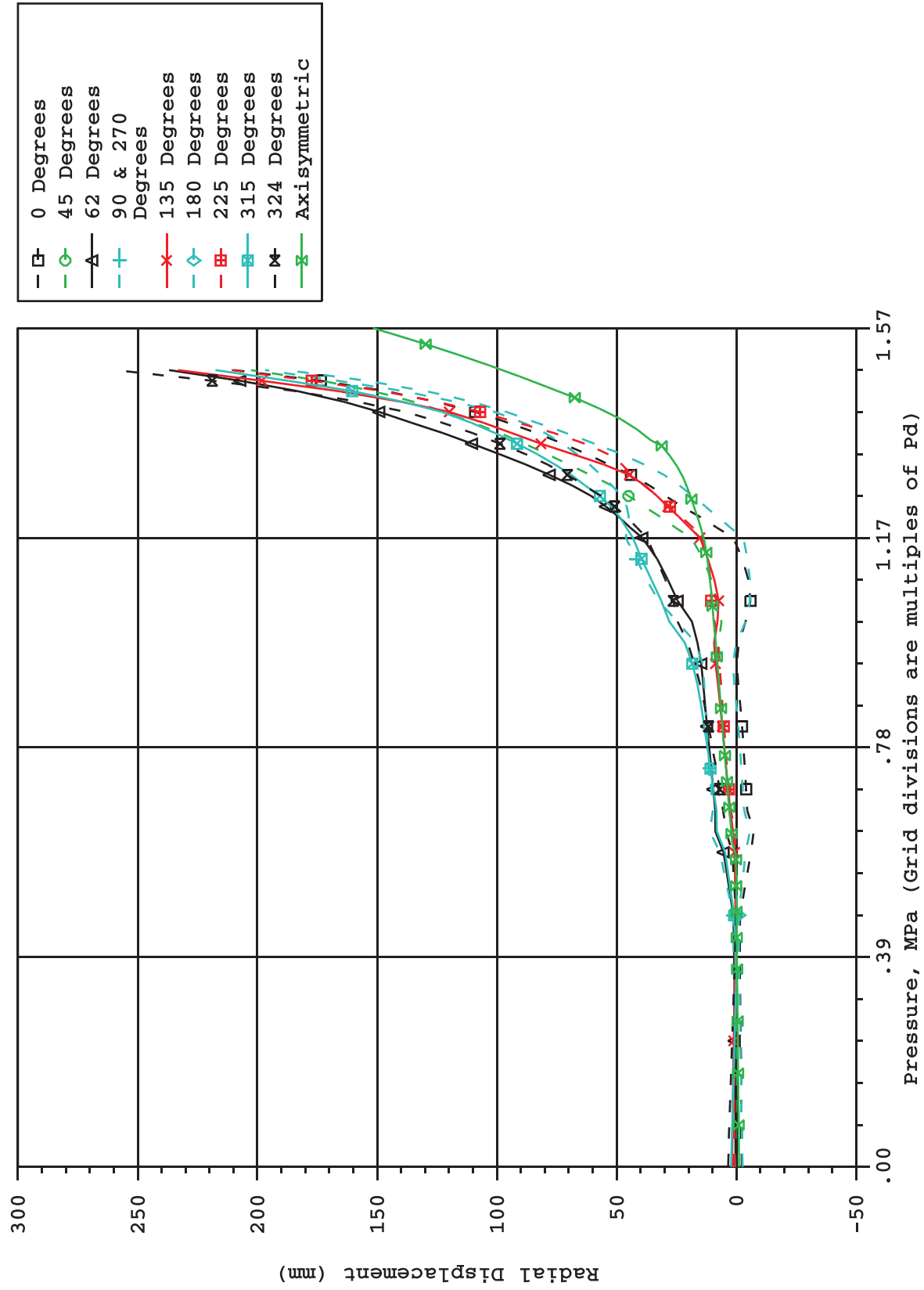   +1.36E+03
    +1.39E+03
C SCALE= 6.89E-3

32

Figure 2-17. Radial Displacement at EL = 4.7 m, 3DCM Compared to Axisymmetric
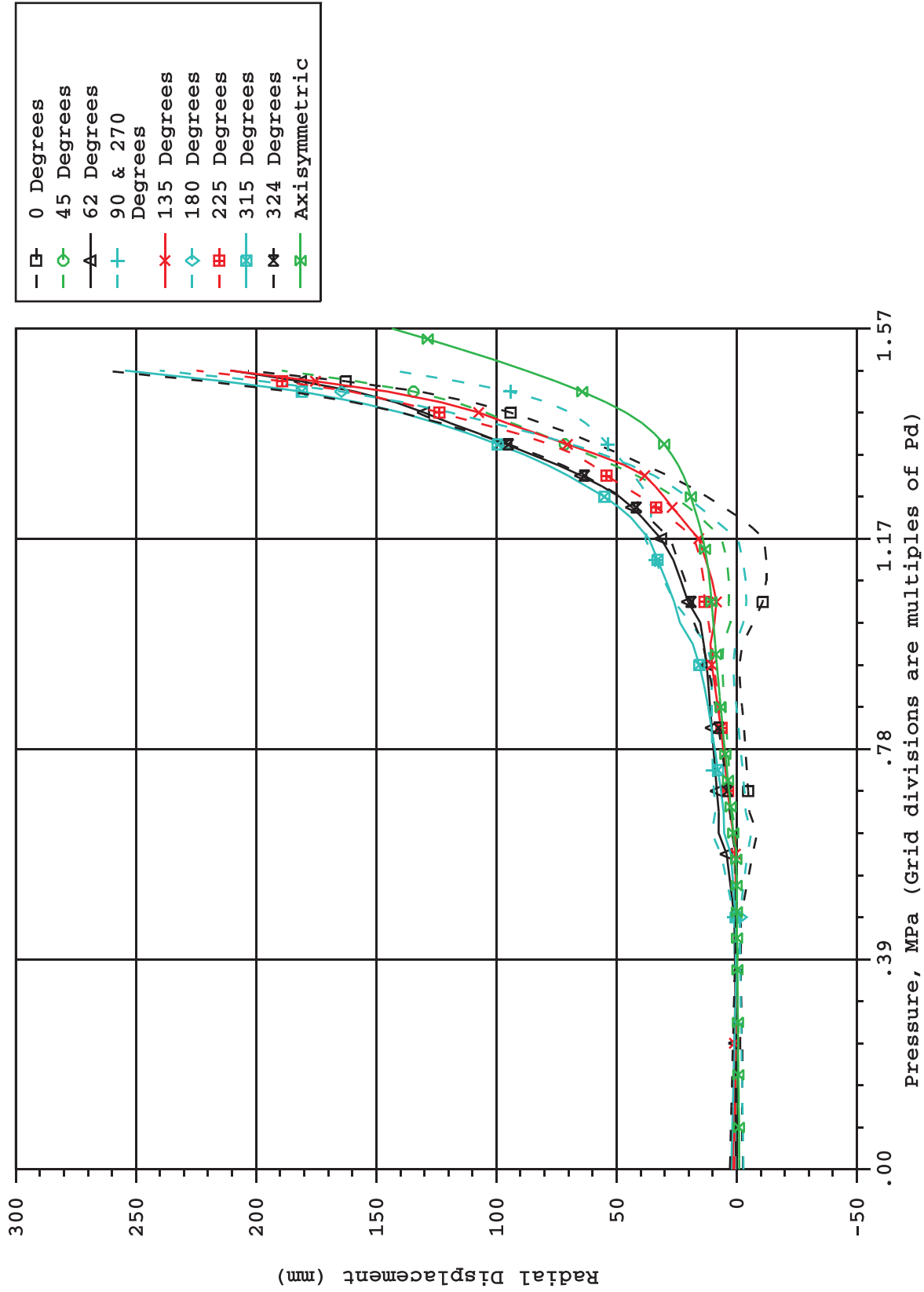
33

Figure 2-18. Radial Displacement at EL = 8.9 m, 3DCM Compared to Axisymmetric